

Should scatter be corrected in both transmission and emission data for accurate quantitation in cardiac SPET?

Georges El Fakhri^{1, 2}, Irène Buvat², Pedro Almeida³, Bernard Bendriem⁴, Andrew Todd-Pokropek², Habib Benali²

¹Department of Radiology, Brigham and Women's Hospital and Harvard Medical School Boston, Massachusetts, USA

²U494 INSERM, CHU Pitié-Salpêtrière, Paris, France

³Serviço de Medicina Nuclear, Hospital Garcia de Orta, Almada, Portugal

⁴CTI, Inc., Knoxville, Tenn., USA

Received 19 January and in revised form 6 May 2000 / Published online: 29 June 2000

© Springer-Verlag 2000

Abstract. Ideally, reliable quantitation in single-photon emission tomography (SPET) requires both emission and transmission data to be scatter free. Although scatter in emission data has been extensively studied, it is not well known how scatter in transmission data affects relative and absolute quantitation in reconstructed images. We studied SPET quantitative accuracy for different amounts of scatter in emission and transmission data using a Utah phantom and a cardiac Data Spectrum phantom including different attenuating media. Acquisitions over 180° were considered and three projection sets were derived: 20% images and Jaszczak and triple-energy-window scatter-corrected projections. Transmission data were acquired using gadolinium-153 line sources in a 90–110 keV window using a narrow or wide scanning window. The transmission scans were performed either simultaneously with the emission acquisition or 24 h later. Transmission maps were reconstructed using filtered backprojection and μ values were linearly scaled from 100 to 140 keV. Attenuation-corrected images were reconstructed using a conjugate gradient minimal residual algorithm. The μ value underestimation varied between 4% with a narrow transmission window in soft tissue and 22% with a wide window in a material simulating bone. Scatter in the emission and transmission data had little effect on the uniformity of activity distribution in the left ventricle wall and in a uniformly hot compartment of the Utah phantom. Correcting the transmission data for scatter had no impact on contrast between a hot and a cold region or on signal-to-noise ratio (SNR) in regions with uniform activity distribution, while correcting the emission data for scatter improved contrast and reduced SNR. For absolute quantitation, the most accurate results (bias <4% in both phantoms) were obtained when reducing scatter in both emission and transmission data. In conclusion, trying to obtain the

same amount of scatter in emission and transmission data, in addition to being impractical because of the difficulty in knowing the precise scatter components, did not yield such accurate absolute activity quantitation as when emission and transmission scatter were reduced.

Key words: Scatter – Transmission computed tomography – Absolute and relative quantitation

Eur J Nucl Med (2000) 27:1356–1364

DOI 10.1007/s002590000304

Introduction

Accurate attenuation compensation in single-photon emission tomography (SPET) requires measurement of the patient-specific attenuation properties. Such measurements can be performed using a transmission computed tomography (TCT) acquisition involving an external source of gamma rays (e.g., [1]). Scatter affects both SPET and TCT measurements. When performing a simultaneous SPET-TCT study in which the emission energy is greater than that of the transmission source (as is usually the case with technetium-99m SPET studies), scatter photons included in the transmission data have two components: downscatter due to photons emitted by the radioactive distribution inside the patient, and scatter due to photons emitted by the transmission source.

Scatter in the transmission data yields an overestimation of the transmitted counts and hence an underestimation of the μ values. Because of this underestimation, attenuation correction does not restore enough counts in the reconstructed slices. This underestimation somewhat offsets the extra counts in the projections due to scatter from the emission source. This is why it has been suggested (e.g., [2], [3]) that attenuation coefficient values smaller than the theoretical values be used (e.g.,

Correspondence to: G. El Fakhri, Department of Radiology, Brigham and Women's Hospital, Boston, MA 02115, USA

0.12 cm⁻¹ instead of 0.15 cm⁻¹ for water) to compensate simultaneously for scatter and attenuation. The purpose of this work was to assess absolute and relative quantitation accuracy when compensating scatter in the emission data by scatter in the transmission data and when correcting both transmission and emission data for scatter. To do so, different configurations involving different amounts of scatter in emission and transmission data were considered for two physical phantoms: a Utah phantom and a Data Spectrum cardiac phantom.

Materials and methods

Phantoms

Utah phantom

The Utah phantom (Fig. 1A) was originally designed for the assessment of the effect of scatter evaluation in positron emission tomography [4]. It consists of a 20-cm-diameter cylinder, 15 cm in length, which includes four compartments labelled from 1 to 4: a 15-cm-long annulus, 2 cm thick, with an outside diameter of 20 cm (compartment 1), an inner cylinder 15 cm long and 16 cm in diameter (compartment 2), a small cylinder 10.5 cm long and 4.5 cm in diameter (compartment 3), and a shorter cylinder 5.5 cm long and 4.5 cm in diameter (compartment 4). A fifth cylindrical compartment (compartment 5), 10 cm long and 20 cm in diameter is attached to one end of the phantom. Compartments 1, 2, and 5 were filled with water ($\mu=0.167$ cm⁻¹ at 100 keV) while compartment 3 was filled with K₂HPO₄ to mimic bone attenuation ($\mu=0.323$ cm⁻¹ at 100 keV [5]) and compartment 4 with NH₄I ($\mu=0.645$ cm⁻¹ at 100 keV [5]). Compartments 1 and 2 were filled with 81.4 MBq (48.0 kBq/ml) and 20 MBq of ^{99m}Tc respectively (8.0 kBq/ml). The other compartments did not contain any radioactive solution.

Cardiac Data Spectrum phantom

A Data Spectrum cardiac phantom (Chapel Hill, NC) was considered (Fig. 1B). The phantom consists of an elliptical 24×32 cm cylinder filled with water, including a left ventricle (LV) compartment with a 10-mm-thick wall filled with water, two lung compartments filled with a mixture of expanded polystyrene and water ($\mu=0.063$ cm⁻¹ at 100 keV), and a Teflon spine (attenuation coefficient similar to bone: $\mu=0.329$ cm⁻¹ at 100 keV). A 530-ml perfusion bag of saline water was added to simulate the liver. The LV wall was filled with 7.96 MBq (72 kBq/ml), to mimic myocardial perfusion in normal patients [6, 7], and the liver was filled with 22 MBq (46 kBq/ml) of ^{99m}Tc.

Emission and transmission studies

Emission imaging

An L-shaped double-headed SMV camera was used. Emission acquisitions were performed over 180° on a circular orbit (radius of rotation: 20 cm) with 64 projections (60 s per projection) and a 128×128 pixel matrix (pixel size: 3.8 mm × 5 mm). Three energy

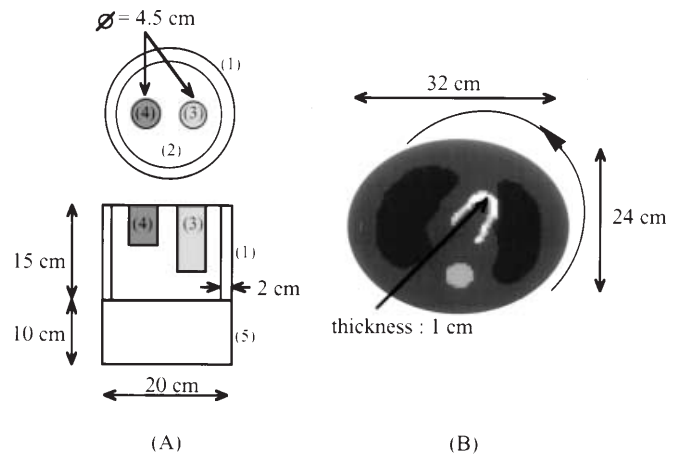


Fig. 1. Transverse slice of the Utah phantom (A) and the cardiac Data Spectrum phantom (B) used

windows were used: [93–122 keV], [123.5–128.5 keV], and [126–154 keV]. For each phantom, two emission acquisitions were performed: a first acquisition was performed with the LV compartment or compartment 1 of the Utah phantom alone in air (scatter and attenuation were thus negligible), in the same position it had in the phantom. A second acquisition was performed using the whole cardiac phantom or Utah phantom, including all compartments.

Transmission imaging

The transmission data were acquired using two gadolinium scanning line sources (100 keV, 2000 MBq) facing the two heads, in a 20% energy window [90–110 keV]. In addition to the collimation of the transmission source by a lead shielding, an electronic scanning window was used to reduce the amount of scattered photons detected during the transmission scans, as proposed by Tan et al. [8]. Two apertures of this scanning window were considered: a 3-cm-wide (W3) and a 10-cm-wide window (W10). Transmission imaging was performed for 30 s per projection, either simultaneously with emission imaging [W3(E+T) or W10(E+T)] or 24 h after the emission scan [W3(T) or W10(T)]. In the simultaneous emission/transmission scans, scatter from ^{99m}Tc activity could contaminate transmission data. In the emission scans performed 24 h (i.e., four half-lives) after emission imaging, there was almost no contamination from ^{99m}Tc activity (residual ^{99m}Tc <1.9 MBq). All transmission studies were performed over 180° using a circular orbit identical to that used for the emission scan.

Data analysis

Emission data

In addition to the 20% energy window [126–154 keV] (I20), two scatter corrections were performed on the emission projections: the Jaszczak subtraction (JAS) and the triple energy window (TEW) correction.

When using the JAS method [9], scatter-corrected images were obtained by subtracting the [93–122 keV] Compton projections, weighted by $k=0.5$, from the I20 projections.

For each projection, the TEW correction [10] estimates the number of scattered photons within the 20% energy window using the number of photons detected in two energy windows I_1 and I_2 , centred on $E_1 = 126$ keV and $E_2 = 154$ keV respectively. Given that the width w of the I20 image was 28 keV, and setting the width of the I_1 image to 5 keV and that of the I_2 image to zero, the scatter-free image I_{TEW} was obtained by [10]:

$$TEW = I20 - \left[\frac{I_1}{w_1} + \frac{I_2}{w_2} \right] \frac{w}{2} = I20 - 2.8I_1.$$

In summary, for each phantom, we had three sets of emission data: the 20% projections I20, the JAS-corrected images and the TEW-corrected images.

Transmission data

For each phantom, the four sets of transmission projections W3(E+T), W10(E+T), W3(T), and W10(T) were reconstructed with filtered backprojection (FBP) (Hann filter, cut-off frequency = 0.5 pixel⁻¹) and linearly scaled from the ¹⁵³Gd energy to the ^{99m}Tc energy using $\mu_{Tc} = 0.9 \mu_{Gd}$ [5].

Image reconstruction

The emission projections of the LV acquired in air and of compartment 1 of the Utah phantom acquired in air were reconstructed using FBP (Hann filter, cut-off frequency = 0.5 pixel⁻¹).

For both phantoms, the I20 emission projections were first reconstructed without attenuation correction using FBP (Hann filter, cut-off frequency = 0.5 pixel⁻¹). The I20, JAS, and TEW emission projections were then reconstructed using an iterative least-square minimal residual algorithm (MR) [11] including nonuniform attenuation correction. The projector modeled nonuniform attenuation using one of the four attenuation maps that were acquired and 20 iterations were performed. Note that MR without attenuation correction is identical to FBP [11]. For each phantom, the reconstruction of the three sets of emission projections I20, JAS, and TEW using the four different attenuation maps yielded 12 reconstructed volumes. In all reconstructed images, the voxel size was 3.8×3.8×5 mm.

Evaluation criteria

Five criteria were considered to characterize the effects of scatter in the emission and transmission scans: (1) the accuracy of the attenuation map values; (2) the image uniformity in regions where activity was theoretically uniform; (3) the contrast between two regions with different activity concentrations; (4) the signal-to-noise ratio in regions where activity was uniformly distributed; (5) the percent bias of the estimated activity with respect to the true activity in specific regions.

Accuracy of the attenuation map values. The four reconstructed transmission maps for each phantom were used to estimate the average attenuation coefficient for each compartment at 100 keV and these coefficients were compared with the theoretical values. Ten measurements were performed in each compartment of each attenuation map, and a mean attenuation coefficient and standard deviation were calculated. Water attenuation coefficient was measured in four compartments corresponding to three different emission-to-transmission ratios: compartment 1 of the Utah phantom

(ratio of 1:25), compartment 2 of the Utah phantom and liver of the cardiac phantom (ratio of 1:100), and LV wall (ratio of 1:250).

Image uniformity. For the Utah phantom, nine volumes of interest (VOIs) were drawn in compartment 1 (75 voxels each) and in compartment 2 (200 voxels each). The mean activity in each region was computed and these nine values were normalized by the same factor so that the highest normalized value was set to 100. The mean of the nine normalized values defined a uniformity index, which should ideally be 100 since activity was uniformly distributed inside compartments 1 and 2.

For the cardiac phantom, the transverse slices were first re-oriented into short-axis slices and bull's eye maps (BEMs) were derived. The BEMs were divided into nine myocardial regions and the mean activity in each region was calculated. The nine resulting values were normalized so that the highest of these nine normalized values was 100. The mean of the nine normalized values defined a BEM uniformity index. As activity was uniformly distributed in the LV wall, the ideal value for the uniformity index was 100.

Contrast. For the Utah phantom, contrast between compartment 2 (theoretical activity concentration of 48 kBq/ml) and compartment 5 (no activity) was considered by drawing a 1800-voxel VOI inside compartment 2 and a 1800-voxel VOI at the same depth inside compartment 5. The mean number of counts m_1 and m_2 in the hot and cold regions respectively were calculated and the contrast was deduced by:

$$C = \frac{m_1 - m_2}{m_1 + m_2}.$$

The ideal contrast value was 1. Contrast was also computed between a 300-voxel VOI drawn inside the compartment 2 near the annulus 1 and a 300-voxel VOI drawn inside compartment 1. Since radioactive concentration was 6 times greater in compartment 1 than in compartment 2 the ideal contrast between the two regions was 0.71.

For the cardiac phantom, the contrast was calculated between a VOI drawn inside the LV wall (1163 voxels, theoretical activity concentration was 72 kBq/ml) and a VOI drawn well inside the LV cavity (1004 voxels, no activity). The ideal contrast value was 1.

Signal-to-noise ratio. A large VOI (2200 voxels) was drawn inside compartment 2 for the Utah phantom and inside the liver (VOI of 1087 voxels) for the cardiac phantom. For each reconstruction, a Kolmogorov-Smirnov test [12] was performed to determine whether the voxel values in the VOI followed a Gaussian distribution. Signal-to-noise ratio was calculated as the ratio of the mean over the standard deviation of the VOI voxel values.

Percent bias in activity. The cross-calibration factor of the gamma camera was determined using a point source acquisition in air (8 kcounts/pixel/MBq). For the Utah phantom, the reference activity that should theoretically be measured in compartment 2 in the absence of scatter and attenuation was then deduced (variable collimator response and partial volume effects were negligible in a large volume such as compartment 2). A 940-voxel VOI was drawn inside compartment 2 and the percent bias in activity estimate was deduced by comparing the estimated activity obtained for each correction scheme with the reference activity.

The mean percent bias affecting activity estimates was also calculated in compartment 1 of the Utah phantom by considering a reference activity distribution that was similarly affected by variable collimator response and partial volume effect (for a 2-cm-thick ring of activity) but not by scatter and attenuation. This reference was obtained from the acquisition of compartment 1 alone

in air (volume \approx 1640 ml), by compensating for scatter using JAS and attenuation using the MR algorithm with an attenuation map of compartment 1 acquired in the absence of ^{99m}Tc activity with a 3-cm-wide scanning window.

For the cardiac phantom, a percent bias in estimated LV wall activity was calculated for each of the nine regions of the BEM by comparing the mean count value with the corresponding number of counts obtained from the acquisition performed in air. As the LV cavity contained only air, the self-attenuation associated with the 1-cm-thick ventricle was considered negligible (volume \approx 110 ml). If scatter and attenuation were properly compensated for in the data affected by attenuation and scatter, these two numbers of counts should be the same and the bias should be zero.

Results

Figure 2 shows a reconstructed slice of the attenuation map obtained with each attenuation setting [W3(E+T), W3(T), W10(E+T), and W10(T)] through the LV of the cardiac Data Spectrum phantom. The corresponding reconstructed transverse slices of I20+MR, JAS+MR, and TEW+MR obtained when performing attenuation correction using each of the four maps are also shown. All images are displayed using the same minimum and maximum of the color scale.

Accuracy of the attenuation map values

The highest local emission-to-transmission count ratio in the cardiac region, measured by comparing count rates in the LV region in W3(E+T) and W3(T) images, was 1.8:100 and that measured by comparing count rates in W10(E+T) and W10(T) images was 2.5:100.

Table 1 shows the attenuation coefficients measured at 100 keV for each transmission scheme for the two phantoms. In lung-equivalent material (expanded polystyrene + water, cardiac phantom), all measured attenuation coefficients were close to the theoretical value [no significant difference (NS) between the measured values and the theoretical value using unpaired Student's *t* tests for $\alpha=0.05$].

In water (Utah and cardiac phantom), the attenuation coefficient values were not significantly different from the theoretical values with the narrower scanning windows [W3(T) or W3(E+T)]. When using the large transmission window [W10(E+T) and W10(T)], however, the μ values were underestimated by about 11% in compartment 2 of the Utah phantom and by up to 16% in the liver of the cardiac phantom with W10(E+T) ($P<0.05$). For a given transmission setting [W3(T), W3(E+T), W10(T), or W10(E+T)], no significant difference was observed between the water attenuation coefficients calculated in the LV and those calculated in the liver regions (NS), or in compartment 1 and in compartment 2 of the Utah phantom (NS). Furthermore, for a given transmission setting, no significant difference (NS) was observed be-

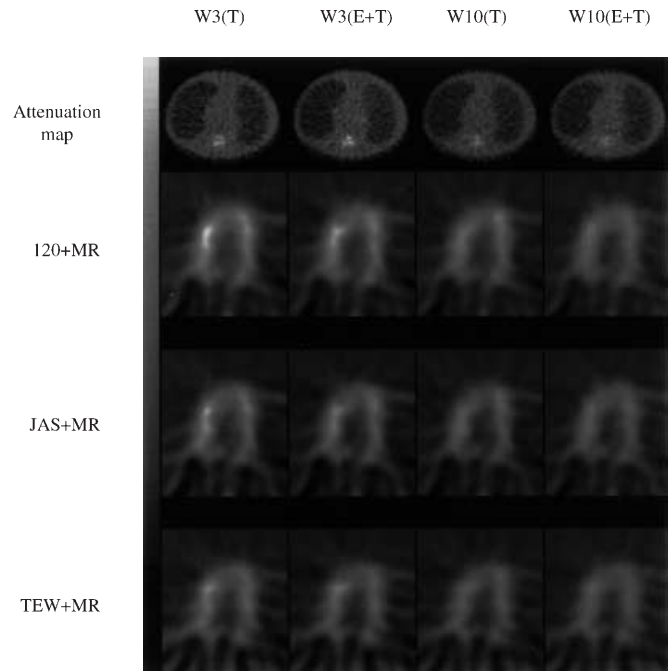


Fig. 2. Reconstructed transverse slices of I20, JAS, and TEW activity distributions through the LV of the cardiac Data Spectrum phantom with the four attenuation maps

Table 1. Attenuation coefficients [μ values (cm^{-1})] measured at 100 keV for each transmission scheme for the two phantoms

	Theoretical	W3(T)	W3(E+T)	W10(T)	W10(E+T)
Utah phantom					
Water cpt 1	0.167	0.164 \pm 0.025	0.151 \pm 0.028	0.153 \pm 0.027	0.147 \pm 0.029*
Water cpt 2	0.167	0.163 \pm 0.022	0.154 \pm 0.024	0.150 \pm 0.026*	0.149 \pm 0.027*
K ₂ HPO ₄	0.323	0.312 \pm 0.031	0.264 \pm 0.035*	0.222 \pm 0.036*	0.220 \pm 0.038*
NH ₄ I	0.645	0.460 \pm 0.036*	0.433 \pm 0.039*	0.354 \pm 0.041*	0.351 \pm 0.044*
Cardiac phantom					
Polystyrene	0.063	0.063 \pm 0.029	0.063 \pm 0.028	0.055 \pm 0.023	0.053 \pm 0.023
Water LV	0.167	0.162 \pm 0.041	0.152 \pm 0.044	0.152 \pm 0.034	0.140 \pm 0.035*
Water liver	0.167	0.161 \pm 0.049	0.155 \pm 0.047	0.150 \pm 0.042*	0.142 \pm 0.042*
Teflon	0.329	0.315 \pm 0.042	0.282 \pm 0.047*	0.267 \pm 0.044*	0.257 \pm 0.040*

*Values that are significantly different ($P<0.05$) from the corresponding theoretical attenuation values

tween the water attenuation coefficients measured in the Utah phantom (compartments 1 or 2) and those measured in the cardiac phantom (LV or liver compartments).

For high μ values (Teflon in the cardiac phantom, K_2HPO_4 and NH_4I in the Utah phantom), the underestimation of the theoretical μ value tended to be larger than for water μ values. In Teflon (theoretical μ of 0.329 cm^{-1}), the underestimation varied between 4% for W3(T) (NS) and 22% with W10(E+T) ($P<0.05$) and in K_2HPO_4 , it varied between 3% (NS) and 32% ($P<0.05$) for W3(T) and W10(E+T) respectively. In NH_4I , the underestimation of the μ value varied between 29% with W3(T) ($P<0.05$) and 46% with W10(E+T) ($P<0.05$).

Overall, the best accuracy in estimating the theoretical μ values at 100 keV was obtained with the narrow transmission window and with the transmission scan sequential to the emission scan [W3(T)], i.e., with the lowest amount of scatter present in the transmission data. The more scatter in the transmission images, the larger the underestimation, and for a given amount of scatter, the greater the theoretical value, the larger the underestimation.

Furthermore, for polystyrene and water, no significant difference at the risk of 5% was observed between measured attenuation coefficients using W3(T) and those measured with W3(E+T) (paired t test). The difference of the values measured for W3(T) and W3(E+T) became significant in Teflon and K_2HPO_4 ($P<0.05$, paired t test). Likewise, no significant difference was observed between measured attenuation coefficients of polystyrene with W3(T) and W10(T). However, a significant difference was observed when measuring attenuation coefficients of water, K_2HPO_4 , and NH_4I with W3(T) as compared with W10(T) ($P<0.05$).

Image uniformity

Attenuation correction significantly improved uniformity in both phantoms. In the Utah phantom, the uniformity of the activity distribution in compartment 1 increased from 80 without attenuation correction (I20+FBP) to 89 when attenuation was corrected using the W3(T) map [denoted as I20+W3(T)] ($P<0.05$). The uniformity of activity distribution in compartment 2 also increased from 84 with I20+FBP to 91 with I20+W3(T) ($P<0.05$) (Table 2). Likewise, the BEM uniformity was significantly improved after attenuation correction [72 with I20+FBP against 88 with I20+W3(T)] ($P<0.05$).

The amount of scatter included in the emission or transmission data had little effect on the uniformity of activity distribution: for both phantoms, there was no definite trend towards better or poorer uniformity when considering the reconstruction of the projections (I20, JAS, or TEW) corrected for attenuation using any of the four attenuation maps [W3(T), W3(E+T), W10(T), or W10(E+T)].

Table 2. Uniformity for compartments 1 and 2 of the Utah phantom and for the BEM in the cardiac phantom (ideal uniformity = 100 for Utah and cardiac phantoms)

	W3(T)	W3(E+T)	W10(T)	W10(E+T)
Utah phantom cpt 1 (I20+FBP: 80)				
I20	89±5	91±5	90±5	89±6
JAS	90±5	90±4	89±4	89±5
TEW	89±6	89±6	88±6	88±6
Utah phantom cpt 2 (I20+FBP: 84)				
I20	91±7	91±6	92±6	92±6
JAS	92±6	92±5	91±4	92±5
TEW	93±5	92±5	92±4	92±5
Cardiac phantom (I20+FBP: 72)				
I20	88±6	88±6	89±5	86±5
JAS	89±6	89±5	87±7	87±6
TEW	89±6	88±6	86±7	87±6

Contrast

The contrast between compartments 2 and 5 of the Utah phantom was 0.69 instead of 1 when no correction was performed (I20+FBP). Correcting for attenuation alone did not significantly improve contrast [0.71 with I20+W3(T)] (Table 3). Likewise, contrast between compartments 1 and 2 was not significantly improved after attenuation correction (0.53 with I20+W3(T) as compared to 0.50 with I20+FBP, NS). Attenuation correction did not significantly improve contrast between the LV wall and cavity in the cardiac phantom (0.68 with I20+FBP and 0.71 with I20+W3(T), NS) either.

In both phantoms, contrast did not significantly increase after reducing scatter in transmission data whatever the scatter content of the emission data. Contrast between compartments 2 and 5 was 0.71 with I20+W3(T) as compared to 0.68 with I20+W10(E+T) (NS). Similarly, contrast between compartments 1 and 2 measured with TEW+W3(T) (0.62) was not significantly different from that measured when using W10(E+T) (0.61, NS). Likewise, contrast between the LV wall and cavity was 0.71 with I20+W3(T) and 0.69 with I20+W10(E+T) (NS). However, contrast significantly increased ($P<0.05$) when emission data were corrected for scatter with either JAS or TEW, and this was true whatever the transmission setting [W3(T), W3(E+T), W10(T), or W10(E+T)]. For the Utah phantom, contrast between compartments 2 and 5 increased from 0.71 with I20+W3(T) to 0.83 with JAS+W3(T) ($P<0.05$) and 0.80 with TEW+W3(T) ($P<0.05$). Contrast between compartments 1 and 2 increased from 0.53 with I20+W3(T) to 0.61 with JAS+W3(T) and 0.62 with TEW+W3(T). Finally, contrast between the LV wall and cavity also increased from 0.71 with I20+W3(T) to 0.79 with JAS or TEW+W3(T) ($P<0.05$).

Table 3. Contrast between compartments 1 and 2 of the Utah phantom, between compartments 2 and 5 of the Utah phantom, and between the LV wall and LV cavity in the cardiac phantom (ideal contrast = 1 for cardiac phantom and between compartments 2 and 5; ideal contrast = 0.71 between compartments 1 and 2)

	W3(T)	W3(E+T)	W10(T)	W10(E+T)
Contrast cpt 1 and 2 (I20+FBP: 0.50)				
I20	0.53±0.11	0.54±0.12	0.52±0.11	0.51±0.10
JAS	0.61±0.08	0.62±0.09	0.61±0.10	0.63±0.14
TEW	0.62±0.12	0.61±0.13	0.60±0.11	0.61±0.13
Contrast cpt 2 and 5 (I20+FBP: 0.69)				
I20	0.71±0.08	0.70±0.09	0.69±0.06	0.68±0.07
JAS	0.83±0.10	0.80±0.09	0.79±0.09	0.78±0.10
TEW	0.80±0.12	0.78±0.11	0.76±0.10	0.77±0.10
Contrast LV wall/cavity (I20+FBP: 0.68)				
I20	0.71±0.11	0.71±0.12	0.71±0.10	0.69±0.12
JAS	0.79±0.13	0.78±0.12	0.78±0.14	0.77±0.13
TEW	0.79±0.16	0.78±0.14	0.78±0.13	0.77±0.15

Table 4. SNR in compartment 2 of the Utah phantom and in the liver of the cardiac phantom

	W3(T)	W3(E+T)	W10(T)	W10(E+T)
Utah phantom (I20+FBP: 3.7)				
I20	6.4±0.4	6.2±0.3	6.4±0.3	6.4±0.3
JAS	4.5±0.5	4.4±0.5	4.7±0.5	4.7±0.5
TEW	4.6±0.7	4.7±0.7	4.6±0.6	4.6±0.6
Cardiac phantom (I20+FBP: 4.7)				
I20	5.2±0.4	5.4±0.4	5.4±0.3	5.6±0.3
JAS	4.1±0.4	4.5±0.5	4.3±0.4	4.4±0.4
TEW	4.1±0.5	3.6±0.6	4.1±0.5	4.3±0.4

Signal-to-noise ratio

When emission data were not corrected for scatter, attenuation correction significantly improved the signal-to-noise ratio (SNR) in compartment 2 of the Utah phantom (SNR increased from 3.7 with I20+FBP to 6.4 with I20+W10(E+T), $P<0.05$) and, to a lesser extent, in the liver compartment of the cardiac phantom [4.7 with I20+FBP against 5.6 with I20+W10(E+T), $P<0.05$] (Table 4).

Reducing scatter in the transmission data had no significant impact on SNR in the reconstructed images of both phantoms. On the other hand, correcting the emission data for scatter reduced significantly the SNR in the reconstructed slices in both phantoms.

Table 5. Bias in absolute activity quantitation (%) in compartments 1 and 2 of the Utah phantom and in the LV wall of the cardiac phantom

	W3(T)	W3(E+T)	W10(T)	W10(E+T)
Utah phantom cpt 1 (I20+FBP: -32%)				
I20	42±14	36±12	28±11	19±9
JAS	-5±5	-7±4	-20±5	-26±5
TEW	-5±6	-9±6	-22±5	-27±6
Utah phantom cpt 2 (I20+FBP: -37%)				
I20	49±12	45±11	31±10	21±10
JAS	-3±6	-6±5	-16±6	-20±5
TEW	-4±7	-7±6	-17±6	-22±6
Cardiac phantom LV wall (I20+FBP: -90%)				
I20	8±6	6±5	-6±5	-11±4
JAS	-1±3	-3±4	-15±4	-19±3
TEW	-2±4	-3±4	-15±5	-19±3

Percent bias in activity

When no correction was performed, the activity was underestimated by 32% with I20+FBP in compartment 1 of the Utah phantom, by 37% in compartment 2 and by 90% in the LV of the cardiac phantom. The accuracy of activity quantitation after attenuation correction alone strongly depended on the amount of scatter present in the transmission and emission data: the bias was 42% and 49% in compartments 1 and 2 of the Utah phantom respectively with I20+W3(T), while it was 19% and 21% with I20+W10(E+T) (Table 5). Likewise, mean percent bias in the LV wall was 8% with I20+W3(T) and -11% with I20+W10(E+T). When correcting the emission data for scatter, the smallest biases were observed when using narrow aperture transmission window and sequential acquisition [W3(T)], i.e., the least scatter in the transmission data: the biases were then -5% in compartment 1, -4% in compartment 2, and -1% in the LV wall.

Discussion

Ideally, both emission and transmission data should be scatter free for reliable quantitation in SPET. The effect of scatter in emission data has already been thoroughly investigated but it is not so well known how scatter in transmission data affects the reconstructed images. The aim of this study was to determine, when activity distributions and attenuation are nonuniform, whether scatter should be corrected in both emission and transmission data in order to achieve accurate absolute (activity bias) and relative quantitation (e.g., contrast, uniformity). We considered two phantoms with different activity and attenuation distributions to study the impact of scatter in emission and transmission data.

Results regarding the underestimation of the attenuation coefficients are consistent with those found in the literature (e.g., [5], [13]): the presence of scatter in the transmission data leads to an underestimation of the attenuation coefficients. Furthermore, the higher the material density, the greater the underestimation of the attenuation coefficient: the underestimation varied between 4% [W3(T)] and 17% [W10(E+T)] in water and 4% [W3(T)] and 22% [W10(E+T)] in bone.

The attenuation coefficients measured from the simultaneous emission/transmission scans [W3(E+T) or W10(E+T)] were not significantly different from those measured when the transmission acquisitions were performed 24 h after the emission acquisitions [W3(T) or W10(T)] for water and polystyrene. This means that, in soft tissue, the effect of downscatter from emission into transmission data is negligible for the geometry of acquisition we considered (two detection heads with a 90° angulation) and for the ratio of the transmission source activity to the emission activity (transmission activity about 100 times greater than emission activity). Furthermore, for a given transmission setting, no significant difference was observed between water attenuation coefficients measured in the LV wall, the liver, or compartment 1 or 2 of the Utah phantom. Therefore, the accuracy of the attenuation map did not vary greatly with the ratio of emission-to-transmission counts present in this study (this ratio varied between 1:25 in compartment 1 of the Utah phantom and 1:250 in the LV wall). Further investigation would be required to assess the impact of the emission-to-transmission ratio on the accuracy of the attenuation coefficients for higher emission count rates.

We studied the biases introduced by scatter in the emission and transmission data in SPET quantitation independently of other possible biases that could also affect quantitative accuracy. Indeed, only scatter and attenuation significantly affect quantitative accuracy in large compartments [14] such as compartment 2 of the Utah phantom. On the other hand, measurement of activity in the LV wall in the cardiac phantom and in compartment 1 of the Utah phantom is affected by scatter, attenuation, depth-dependent collimator response, and partial volume effect [14]. However, the activity measured in the LV wall and in compartment 1 of the Utah phantom from the acquisitions performed in air was similarly affected by depth-dependent collimator response as in the acquisitions performed using the whole phantoms. Therefore, comparing measurements from the whole phantoms after scatter and attenuation correction with those from the LV compartment in air or from compartment 1 in air (after MR+JAS) allowed us to assess the impact of scatter and attenuation independently from variable collimator response, assuming that variable collimator response and attenuation can be modeled as separable phenomena [15]. Furthermore, as self-attenuation was negligible in the LV (1-cm-thick wall with a volume of 110 ml), the LV air acquisition yielded the

activity distribution that should be expected from the acquisition of the whole phantom if the scatter and attenuation corrections were accurate. For compartment 1 of the Utah phantom, self-attenuation and scatter due to the 2-cm-thick wall ring (volume \approx 1640 ml) were much less than attenuation and scatter observed for the whole phantom, but non-negligible. We therefore used JAS+MR for scatter and attenuation corrections and assumed that these corrections were accurate enough to yield the reference activity distribution that would be obtained in the absence of scatter and attenuation.

For both phantoms, uniformity as measured in this study characterized the accuracy of relative quantitation between several equally hot regions. As could be expected, attenuation correction significantly increased uniformity in both phantoms. This is consistent with the results of Prvulovich et al. [16], which showed that in patients with low likelihood of coronary artery disease, uniformity of tracer distribution improved after attenuation correction only. Furthermore, when considering a hot region with uniform activity (compartment 2 in the Utah phantom or the LV wall in the cardiac phantom), scattered counts emitted outside this region and detected in the region are roughly compensated by scattered photons emitted in this region and detected elsewhere; hence scatter correction of emission data had a small impact on image uniformity. Some authors have reported that scatter in the emission data may affect BEM uniformity (e.g., [17], [18]). Our cardiac phantom did not show such an effect since the LV and liver compartments were 10 cm apart [14]. Furthermore, uniformity of activity distribution was not affected by the ratio of emission-to-transmission counts since it was not significantly different, for a given transmission setting, between regions corresponding to different emission-to-transmission activity ratios (1:25 in compartment 1 of the Utah phantom, 1:100 in compartment 2 of the Utah phantom, 1:250 in the LV wall).

Our results show that emission counts downscattering in the transmission window did not significantly affect the estimation of attenuation coefficients in water and lung-equivalent materials. Therefore, since the cardiac phantom was essentially composed of these materials, and as attenuation correction had the major impact on uniformity of activity distribution, reducing scatter in the transmission data did not significantly affect uniformity. Moreover, since the LV had a uniform attenuation coefficient equivalent to water, underestimation due to scatter in the transmission data led to a uniform underestimation of LV attenuation coefficient and therefore did not affect uniformity of activity distribution.

Correcting for attenuation did not significantly improve contrast between a hot and a cold region (compartments 2 and 5 in the Utah phantom, LV wall and cavity in the cardiac phantom). This is because, in both phantoms, the regions used to measure contrast were close and contained the same attenuating media (water). There-

fore attenuation correction had a similar effect on the two regions involved in contrast assessment.

Reducing scatter in transmission data had no impact on contrast between a hot and a cold region (compartments 2 and 5 of the Utah phantom and LV wall and LV cavity of the cardiac phantom), or between two regions with different activity concentrations (compartments 1 and 2). This is because reducing scatter in the attenuation map increased uniformly the value of the attenuation coefficient in uniformly attenuating regions. However, compensating the emission data for scatter significantly increased contrast between a "hot" and a "cold" region in both phantoms (by 20% and 13% in the Utah and cardiac phantoms respectively, $P < 0.05$). This is because scattered ^{99m}Tc photons that are detected outside a hot region are not "replaced" by scattered photons emitted from neighboring regions, since the neighboring regions are cold. Hence scatter correction of the emission data is essential to restore contrast between regions with different activity concentrations.

Attenuation correction significantly increased SNR (20% increase in the cardiac phantom, $P < 0.05$) while reducing scatter in transmission data had no impact on SNR in the reconstructed images. On the other hand, correcting the emission data for scatter significantly reduced SNR in the emission data (29% and 21% reduction of SNR with the Utah and cardiac phantoms respectively, $P < 0.05$). This is due to the scatter correction process, which intrinsically amplifies noise by removing counts. The SNR deterioration associated with scatter correction could be improved by smoothing scatter projections before subtraction or by incorporating scatter in the reconstruction model as proposed by King et al. [19].

Finally, the major effect of scatter in emission and transmission data concerned accuracy of activity quantitation. When scatter was not corrected for in the emission data, the quantitative biases obtained varied between 19% and 49% for the Utah phantom and between -11% and 8% for the cardiac phantom depending on the emission-to-transmission ratio and the scatter content of emission data as well as that of transmission data. When scatter was made the lowest possible in both emission and transmission data, quantitative biases were less than 5% in both phantoms.

Conclusion

By studying 24 different configurations of scatter in emission and transmission data, we found that reducing scatter in both emission and transmission data yielded the best accuracy in terms of absolute activity estimates in different compartments. However, this was at the expense of the signal-to-noise ratio, which was significantly reduced when emission data were corrected for scatter. Also, we found that in regions with a uniform

activity distribution, the amount of scatter in the emission and in the transmission data had little effect on the uniformity of the restored activity distribution.

When the amount of scatter in the transmission data was locally about the same as the amount of scatter in the emission data, absolute activity could be accurately estimated locally. However, relative quantitation was biased since scatter in the emission data always reduced contrast. Therefore, when accurate absolute and relative quantitations are of interest, both emission and transmission data have to be compensated for scatter.

Acknowledgements. This work was supported in part by grants from SMVI, the "Institut de Formation Supérieure Biomédicale" (Villejuif, France), and the Portuguese government (PRAXIS-XXI/BD3300/94).

References

- Bailey DL. Transmission scanning in emission tomography. *Eur J Nucl Med* 1998; 25: 774–787.
- Jaszczak RJ, Coleman RE, Whitehead FR. Physical factors affecting quantitative measurements using camera-based single photon emission computed tomography (SPECT). *IEEE Trans Nucl Sci* 1981; 28: 69–80.
- Harris CC, Greer KL, Jaszczak RJ, et al. Tc-99m attenuation coefficients in water-filled phantoms determined with gamma cameras. *Med Phys* 1984; 11: 681–685.
- Townsend DW, Choi Y, Sashin D, Minton MA. An investigation of practical scatter correction techniques for 3D PET. *J Nucl Med* 1994; 35: 50P.
- De Dreuille O, Strijckmans V, Almeida P, Loc'h C, Bendriem B. Bone equivalent liquid solution to assess accuracy of transmission measurements in SPECT and PET. *IEEE Trans Nucl Sci* 1997; 44: 1186–1190.
- Diwakar J. Technetium-99m labeled myocardial perfusion imaging agents. *Semin Nucl Med* 1999; 29: 221–236.
- Wackers F, Berman D, Maddahi J, et al. Technetium-99m hexakis-2-methoxyisobutyl isonitrile: human biodistribution, dosimetry, safety, and preliminary comparison to thallium-201 for myocardial perfusion imaging. *J Nucl Med* 1989; 30: 301–311.
- Tan P, Bailey DL, Meikle SR, et al. A scanning line source for simultaneous emission and transmission measurements in SPECT. *J Nucl Med* 1993; 34: 1752–1760.
- Jaszczak RJ, Floyd CE, Coleman RE. Scatter compensation techniques for SPECT. *IEEE Trans Nucl Sci* 1985; 32: 786–793.
- Ogawa K, Hareta Y, Ichihara T, Kubo A, Hashimoto S. A practical method for position-dependent Compton-scatter correction in SPECT. *IEEE Trans Med Imaging* 1991; 10: 408–412.
- La V, Grangeat P. Minimal residual cone-beam reconstruction with attenuation correction in SPECT. *Phys Med Biol* 1998; 43: 715–727.
- Siegel S, Castellan NJ. *Nonparametric statistics for the behavioral sciences*. New York: McGraw-Hill, 1988.
- Frey EC, Tsui BMW, Perry JR. Simultaneous acquisition of emission and transmission data for improved thallium-201 cardiac SPECT imaging using a technetium-99m transmission source. *J Nucl Med* 1992; 33: 2238–2245.

14. El Fakhri G, Buvat I, Péligrini M, et al. Respective roles of scatter, attenuation, collimator response and partial volume effect in cardiac SPECT quantitation: a Monte Carlo study. *Eur J Nucl Med* 1999; 26: 437–446.
15. Glick SJ, Penney BC, King MA, Byrne CL. Noniterative compensation for the distance-dependent detector response and photon attenuation in SPECT imaging. *IEEE Trans Med Imaging* 1994; 13: 363–374.
16. Prvulovich EM, Lonn AH, Bomanji JB, Jarritt PH, Ell PJ. Effect of attenuation correction on myocardial thallium-201 distribution in patients with a low likelihood of coronary artery disease. *Eur J Nucl Med* 1997; 24: 266–275.
17. King MA, Tsui BMW, Pan TS. Attenuation compensation for cardiac single-photon emission computed tomographic imaging. Part 1. Impact of attenuation and methods of estimating attenuation maps. *J Nucl Cardiol* 1995; 2: 513–524.
18. Luo D, King MA, Morgan HT, et al. Investigations into possible causes of hot inferior wall artifacts in attenuation corrected cardiac perfusion images. *IEEE Trans Nucl Sci* 1997; 44: 1146–1153.
19. King MA, Hademenos GJ, Glick SJ. A dual-photopeak window method for scatter correction. *J Nucl Med* 1992; 33: 605–612.